Appl Nanosci (2015) 5:787–794
DOI 10.1007/s13204-014-0379-1

ORIGINAL ARTICLE

Comparison of physical and electrochemical properties of ZnO prepared via different surfactant-assisted precipitation routes

Arun Gupta · Pankaj Srivastava · Lal Bahadur · D. P. Amalnerkar · Ratna Chauhan

Received: 18 July 2014 / Accepted: 10 November 2014 / Published online: 28 November 2014

Abstract The flakes-, hexagons-, nanoparticle-, and flower-like ZnO nanostructures have been synthesized via different surfactant-assisted precipitation routes. The XRD of all ZnO nanostructures is hexagonal single crystalline in nature and the UV–Vis absorption spectra showed blue shift in wavelength corresponding to bulk. The synthesized zinc-oxide nanopowders were used to fabricate dye solar cells sensitized by N719 dye. The comparative study of cells prepared by above ZnO nanopowders has been done. The highest conversion efficiency (2.48 %) for the cell is shown by flower-like ZnO than the others. The difference in photovoltaic parameters for the ZnO nanopowders is due to the difference in surfactants which directly correlate with surface area and dye loading.

Keywords Surfactants · ZnO · N719 dye · Dye-sensitized solar cells

Introduction

Dye-sensitized solar cells (DSSCs) are one of the most promising candidates for future green energy alternative due to their facile, low-cost, and environmentally friendly fabrication process (O'Regan and Gratzel 1991; Zhang and Cao 2011; Duong et al. 2013; Xu et al. 2013). The DSSC assembly consists of dye-fabricated semiconductor oxide electrode sandwiched with platinum electrode in face-to-face manner; the space between the electrodes is filled with electrolyte-containing redox couple. Sandwich-type DSSC assembly has four major parts: oxide semiconductor, photosensitizers, redox couple, and counter electrode. By altering any one of these moieties, the cell parameters such as conversion efficiency, short-circuit current, open-circuit potential, and fill factor parameters can be tuned. Oxide semiconductors are preferentially used in solar cell because of their high stability against photocorrosion on optical excitation in the band gap (Hagfeldt and Grätzel 1995). The large band gap (>3 eV) of the oxide semiconductor is desired in DSSCs for the transparency of the semiconductor electrode for harvesting the solar energy into large spectrum. TiO_2, ZnO, WO_3, Fe_2O_3, SnO_2, Nb_2O_5, and Ta_2O_5 (Hagfeldt and Grätzel 1995) are used as porous nanocrystalline structure in DSSCs. Out of these oxides, TiO_2 is still in demand due to its better performance as high surface area for dye penetration and attracted major attention for their use as semiconductor in dye-sensitized solar cells (Hagfeldt and Grätzel 1995; Kalyansundaram and Grätzel 1998; Kong et al. 2007; Gratzel 2003; Polo et al. 2004; Hagfeldt et al. 2010). However, the natural drawbacks of the conventional TiO_2 nanoparticle photoanode are numerous grain boundaries existing in the film and the slow electron mobility of TiO_2 as compared with other materials such as ZnO and SnO_2 (Hagfeldt and Grätzel 1995; Kalyansundaram and Grätzel 1998; Kong et al. 2007; Gratzel 2003). These drawbacks could result in a high recombination loss and slow electron transport, preventing further increment of the power conversion efficiency (PCE) for TiO2-based DSSCs. The ZnO oxide semiconductor can also be fabricated as photoanode due to its similar band gap level and higher electron mobility ($\sim$115–155 $cm^2\ V^{-1}\ s^{-1}$) with respect to TiO_2 (Zhang

A. Gupta · P. Srivastava · L. Bahadur
Department of Chemistry, Banaras Hindu University, Varanasi 221005, UP, India

D. P. Amalnerkar · R. Chauhan (✉)
Centre for Materials for Electronics Technologies, Panchwati, Off Pashan Road, Pune 411008, India
e-mail: ratnasingh.bhu@gmail.com

et al. 2009; Xu and Sun 2011; Hu et al. 2012; Sakai et al. 2013).

Recently, ZnO-based DSSCs have triggered considerable interest because ZnO has similar band gap level and higher electron mobility with respect to TiO_2 (Polo et al. 2004; Hagfeldt et al. 2010; Zhang et al. 2009; Xu and Sun 2011). Among the various ZnO nanostructures, ZnO nanowire (NW) arrays have been suggested to be a promising photoelectrode configuration because they can provide a direct pathway for rapid electron transport (Hu et al. 2012; Sakai et al. 2013; Meng et al. 2005).

Many investigations have been carried out to synthesize ZnO nanoparticles via different techniques (Meng et al. 2005; Umar et al. 2005; Pan et al. 2001; Wahab et al. 2007a, b, 2008; Meulenkamp 1998; Spanhel and Anderson 1991; Zhang et al. 2002; Nyffenegger et al. 1998; Brinker and Scherer 1990) such as sol–gel technique (Meulenkamp 1998; Spanhel and Anderson 1991), hydrothermal (Zhang et al. 2002), and electrochemical techniques (Nyffenegger et al. 1998). Among these techniques, sol–gel technique is very attractive because it is relatively easy to achieve and allows us to tailor the morphology of the particles by controlling the rate of hydrolysis and condensation reactions (Brinker and Scherer 1990). Among all methods, precipitation and sol–gel technique provides suitable control of nucleation, aging, and growth of particles in solution. The direct precipitation is also one of the simple and cost-effective methods for bulk production of materials (Wahab et al. 2008). In this method, particle growth owes to interact between different aqueous solutions, and therefore very small particles are formed. Tiny size particles with lower solubility product dissolve and re-precipitate on the surface of larger particles in solution; consequently agglomeration takes place in solution as the particles clog together to minimize surface energy (Meulenkamp 1998).

In this paper, a simple and cost-effective precipitation method was used to synthesize ZnO nanoparticles using different surfactants (triethylamine, diethylamine, PEG 6000, and PEG 8000) as a precipitating agent. The synthesized ZnO powders were employed as photoanode sensitized with N719 dye in DSSC and measured the photovoltaic parameters (short-circuit current, open-circuit voltage, fill factor, and cell efficiency).

Experimental

Materials

Zinc acetate (Merck), triethylamine (Merck), diethylamine (Merck), polyethyleneglycol 6000 (Merck), polyethyleneglycol 8000 (Merck), and Ethanol (Merck) were used as received for preparing ZnO powder. For electrolytic solution, acetonitrile (Merck) was used as the medium of electrolyte; LiI (Aldrich) and I_2 (BDH) were used as redox couple in electrolyte without any further purification. Platinum catalyst (T/SP) as counter electrode, the sealing agent (SX1170-60, 50 μm) for packing the assembly, and N719 dye used as photosensitizer in this experiment, all were purchased from Solaronix. Conductive glass plate (15 Ω/cm^2) was obtained from Pilkington, USA.

Preparation of ZnO powder

Zinc acetate (5 mmol, 1.0 g) was dissolved in ethanol (50 mL) with constant stirring for 1 h at 80 °C. Subsequently, triethylamine (2 mmol, 0.5 mL), diethylamine (2 mmol, 0.36 mL), PEG 6000 (0.2 g), and PEG 8000 (0.2 g) were added into this solution with constant stirring for 8 h at 80–90 °C to obtain a white precipitate which was filtered and washed with water and ethanol. The as-prepared powder was dried in air and annealed at 450 °C and coded as Z-1 (triethylamine), Z-2 (diethylamine), Z-3 (PEG 6000), and Z-4 (PEG 8000) (Scheme 1).

Preparation of ZnO electrode (photoanode) and counter electrode

The ZnO photoanode was prepared by making the paste of ZnO powders with ethanol. The paste was spread on conductive glass plate using doctor's blade technique and annealed at 450 °C for half an hour in air. A thin film of

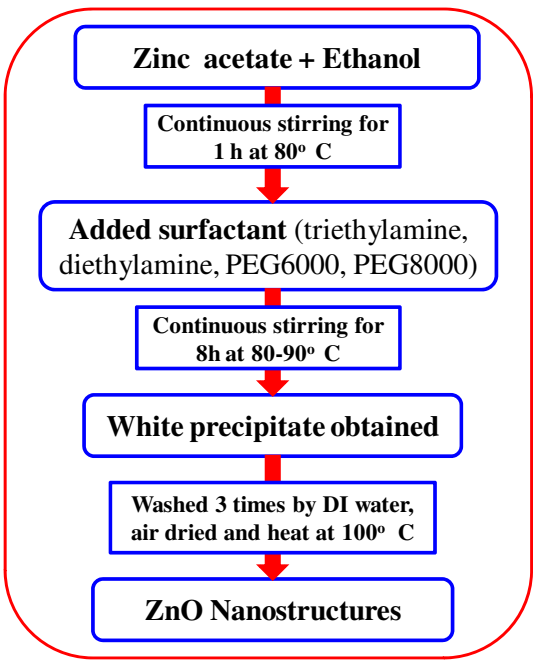

Scheme 1 Flow chart of synthesis procedure of ZnO powders

~5 μm thickness was obtained. The photosensitizer (N719 dye) was adsorbed onto the ZnO surface by dipping the ZnO thin film in an ethanolic solution of N719 dye for 8 h. The non-adsorbed dye was washed off with anhydrous ethanol. The platinum counter electrode was prepared by deposition of Pt catalyst (T/SP paste, Solaronix SA) using screen printing method on conductive glass plate and annealing at 400 °C for half an hour in air.

DSSC assembly

For sandwich-type DSSC assembly, dye-modified ZnO photoanode and platinum-coated counter electrode were positioned over each other in face-to-face sandwich manner leaving the space for making contact, to connect with external load. This assembly was sealed from three sides using the spacer leaving one side open through which the electrolyte solution (0.05 M iodine, 0.5 M LiI and 0.5 M 4-tert. butylpyridine in acetonitrile) was injected into the space between the electrodes. After electrolyte injection, the open side of the cell assembly was also sealed. Copper wires were fixed on both the electrodes using silver paste and araldite for getting electrical contact.

Instrumentation and characterization

The synthesized ZnO powder was characterized by pXRD using X-ray diffractometer (XRD, Bruker AXS model D-8 equipped with a monochromator and Ni-filtered Cu Ka radiation), field emission scanning electron microscope (FESEM, Hitachi S-4800), and UV–Vis (Shimadzu UV–Vis–NIR spectrophotometer-Model UV-3600).

The photoelectrochemical performance, including the short-circuit current (J_{sc}, mA cm^{-2}), open-circuit voltage (V_{oc}, V), fill factor (ff), and overall energy conversion efficiency (η) was determined from the *J–V* curve obtained using a digital Keithley 236 mm under an irradiation of white light from a 1,000 W/HS Xenon arc lamp with a 100 mW cm^{-2} light intensity.

The incident photon-to-electron conversion efficiency (IPCE) measured using a 300 W Xe lamp light source joined to a monochromator (Oriel). A reference Si photodiode calibrated for spectral response was used for the monochromatic power-density calibration.

The electrochemical impedance spectroscopy (EIS) was performed on a CH 660C electrochemical analyzer (CH Instruments, Shanghai, China) in a two electrode configurations. The photoanode was used as a working electrode and the Pt electrode as a counter electrode. The electron transport properties were investigated using electrochemical impedance spectroscopy (EIS) with 10 mV alternative signal in the frequency range of 10^{-2} to 10^{5} Hz.

Result and discussion

UV–Vis spectrum and band gap energy

The absorption spectrum of the ZnO nanostructures is shown in Fig. 1. The band position at 373, 372, 365, and 366 nm corresponding to flakes-like (Z-1), hexagon-like (Z-2), particle-like (Z-3), and flower-like (Z-4) ZnO nanostructures was observed. The blue shift in the ZnO nanostructures, comparing to bulk ZnO (380 nm) is observed due to the size quantization effect (Koch et al. 1985). It is clear that the absorption edge systematically shifts to the lower wavelength or higher energy with decreasing size of the nanoparticle. This definite and orderly shift in the absorption edge is due to the quantum size effect. The flakes-like (Z-1) and hexagon-like (Z-2) ZnO have larger particle size than the others, which was reflected in the absorption spectrum.

X-ray diffraction pattern

Figure 2 shows the XRD pattern of ZnO nanocrystals. The diffraction peaks indicate the nanocrystalline nature with scattering angles (2θ) of 31.72, 34.42, 36.24, 47.49, 56.53, 62.81, 66.28, 67.86, and 68.99 corresponding to the reflection from 100, 002, 101,102, 110, 103, 200, 112, and 201 crystal planes, respectively. The XRD pattern is identical to the hexagonal phase with Wurtzite structure with space group (C6V = $P6_{3mc}$) and unit cell parameters a = b = 3.253 Å and c = 5.2 Å (JCPDS File No. 80-0075).

FTIR spectra

Figure 3 shows the spectrum of the ZnO powders (Z-1 to Z-4) after annealing (450 °C). Only ZnO vibrations at ca.

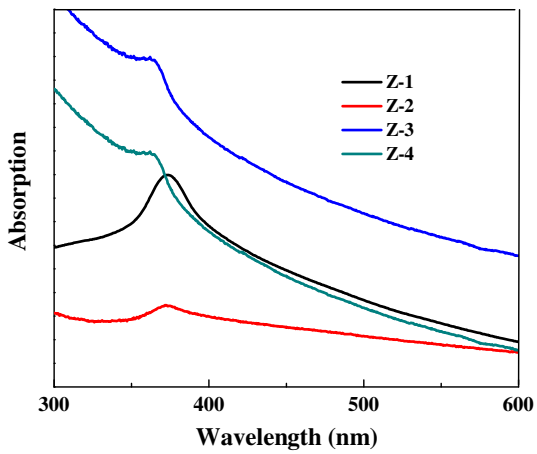

Fig. 1 UV–Vis spectra of different ZnO powders

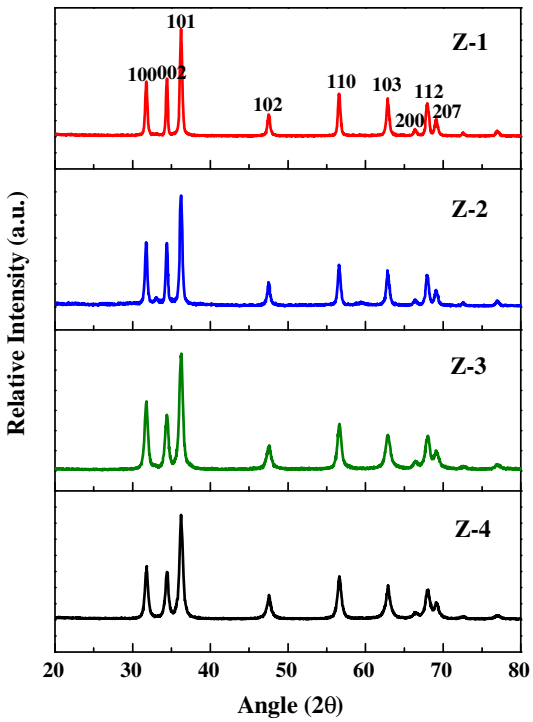

Fig. 2 X-ray diffraction pattern of the different ZnO powders (Z-1 to Z-4); JCPDS file no. 80-0075)

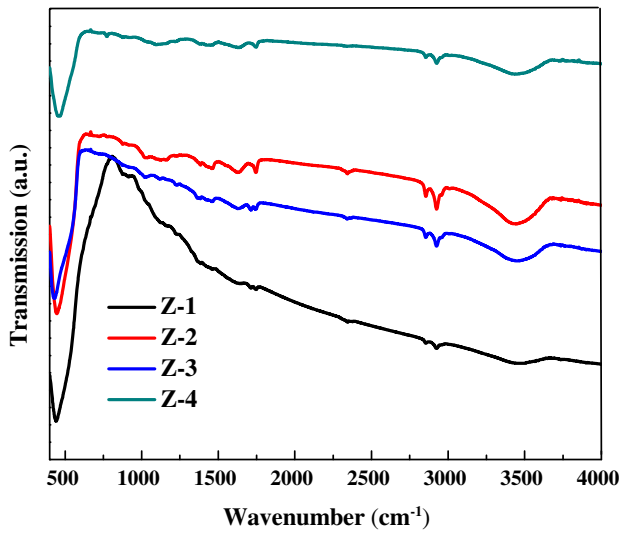

Fig. 3 FTIR spectra for different ZnO powders

490 cm^{-1} are observed indicating that the nanopowders consists of pure ZnO without carbon rests. The large absorption bands at 3,200–3,600 cm^{-1} are assigned to the OH-stretching frequencies of alcohol.

Field emission scanning electron microscopy

The FESEM images of the ZnO nanostructures are shown in Fig. 4. The flakes-like, hexagon-like, particle-like, and flower-like morphologies have been obtained by different surfactant-assisted hydrothermal syntheses. The FESEM image of Z-2a and Z-2b shows the hexagons having small particles grow on the surface which helps to increase the surface area for sufficient dye penetration.

The evaluations of surface area available for dye adsorption for the ZnO powders were investigated by measuring the loading of N719 via desorption experiments (Jennings et al. 2008). Table 1 shows the dye-loading amount for the ZnO powders prepared using different surfactants. The maximum dye loading was shown by Z-3 (particle-like) and Z-4 (flower-like) samples than the Z-1 (flakes-like) and Z-2 (hexagons), due to its greater surface area.

Current–potential (*J–V*) curve

For obtaining *J–V* curve, the data were recorded under solar irradiation by changing the external load from zero (short-circuit conditions) to infinite load (open-circuit conditions). The DSSC assembly was packed using ZnO powders (Z-1 to Z-4) as photoanode sensitized by N719 dye to evaluate their photovoltaic performance (maximum output power, fill factor, and power conversion efficiency) at 100 mW cm^{-2} light intensity. The maximum power (P_{max}) was obtained by choosing a point on *J–V* curve corresponding to which the product of current (J_{max}) and voltage (V_{max}) is maximum. The power conversion efficiency (η) and fill factor (FF) were evaluated using the following relations and

$$\mathrm{FF} = \frac{J_{\max}(A\ \mathrm{cm}^{-2}) \times V_{\max}(V)}{J_{\mathrm{SC}}(A\ \mathrm{cm}^{-2}) \times V_{OC}(V)}, \quad (1)$$

$$\eta(\%) = \frac{J_{\mathrm{SC}} \times V_{\mathrm{OC}} \times FF}{I_{\mathrm{inc}}(W\ \mathrm{cm}^{-2})} \times 100, \quad (2)$$

here, J_{sc}, V_{oc}, and I_{inc} are short-circuit photocurrent, open-circuit potential, and intensity of incident light, respectively. The photocurrent–potential curves for the cell assemblies are shown in Fig. 5.

The photovoltaic performances have been summarized in Table 1 for the cell fabricated using prepared ZnO (Z-1 to Z-2) as photoanode modulated with N719 dye in DSSC assembly. The results show the marked efficiency difference between the cell assemblies fabricated by using different ZnO powders as photoanode. In comparison to Z-1 (1.06 %), Z-4 shows almost double efficiency (2.48 %) with the use of polyethyleneglycol 8000 as surfactant having flower-like morphology. The efficiencies difference between the ZnO powders is mainly due to its difference in surface area. The greater surface area enhances the greater dye loading which facilitates the improvement in cell efficiency.

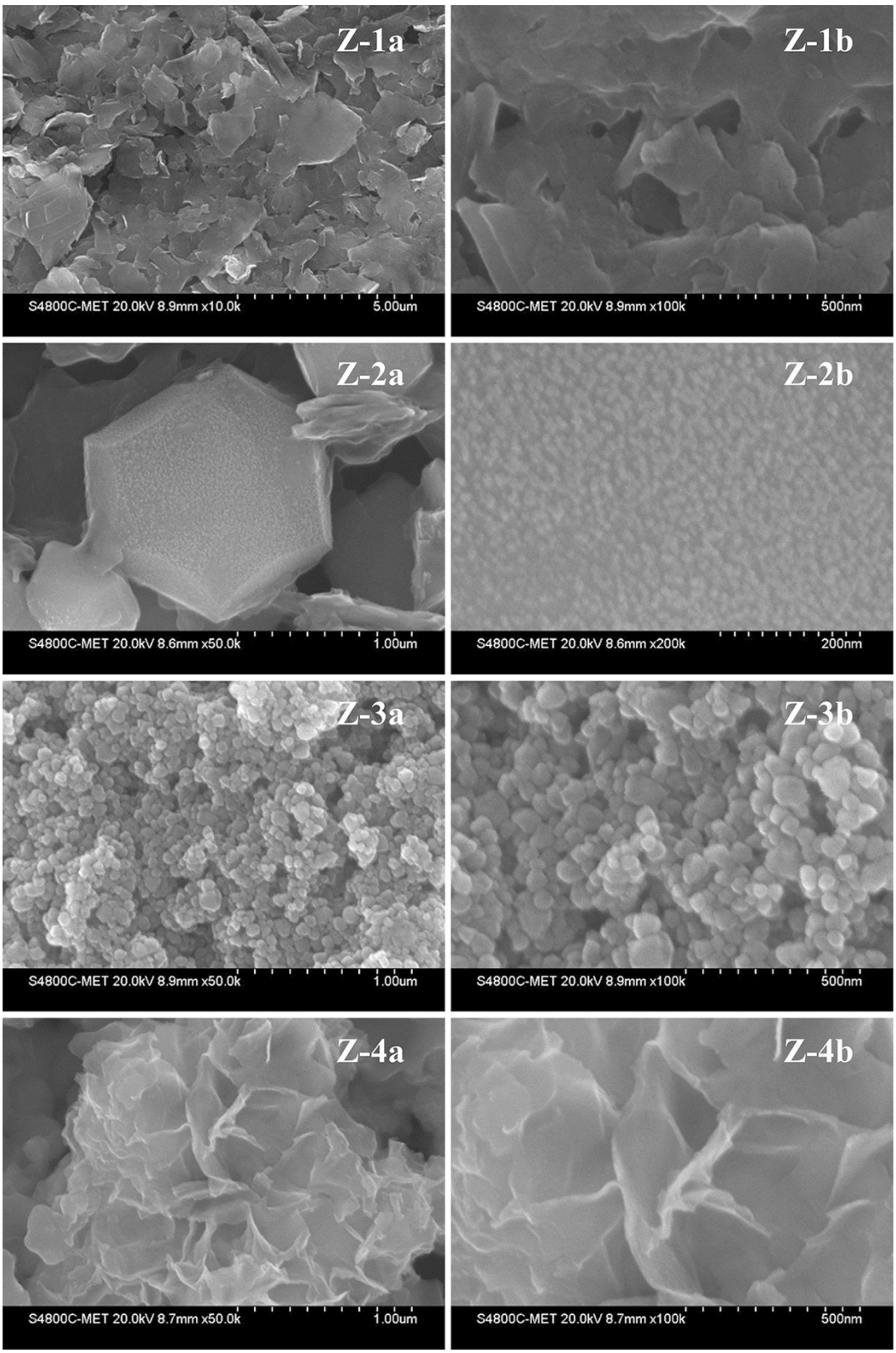

Fig. 4 Typical FESEM images of ZnO nanostructures Z-1(flakes-like), Z-2 (hexagon-like), Z-3 (particle-like), and Z-4 (flower-like) at different magnifications

Table 1 The dye-loading amount and photovoltaic parameters derived from the *J–V* curves shown in Fig. 5

	Dye loading (mol/cm^2)	J_{sc} (mA cm^{-2})	V_{oc} (V)	FF	η (%)	IPCE (%)
Z-1	1.36×10^{-7}	2.77	−0.560	0.68	1.06	36
Z-2	1.56×10^{-7}	3.66	−0.585	0.70	1.50	39
Z-3	1.87×10^{-7}	4.81	−0.600	0.66	1.91	42
Z-4	1.99×10^{-7}	5.62	−0.626	0.69	2.48	46

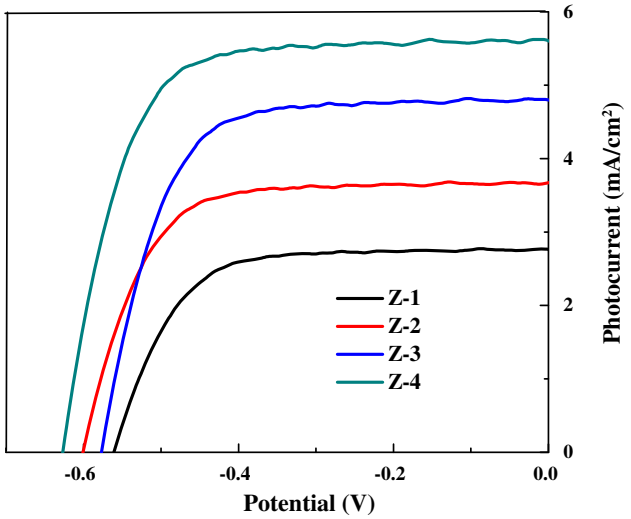

Fig. 5 Photocurrent-potential curves of the DSSCs fabricated with different ZnO powders as photoanode sensitized by N719 dye, illuminated with 100 mW cm^{-2} light intensity

Incident photon-to-current conversion efficiency (*IPCE*)

To determine the ratio of photons that generate electrons in the external circuit to incident photons of monochromatic light is incident photon-to-current efficiency (IPCE) or external quantum efficiency (EQE) for the cell. To quantify the IPCE values, the short-circuit photocurrent (J_{sc}) of the dye-sensitized cell was determined in monochromatic light from 400 to 700 nm. From the values of J_{sc} and the intensity of the corresponding monochromatic light (I_{inc}), the IPCE was calculated at each excitation wavelength (λ) using the following relation:

$$\text{IPCE} = \frac{1240 \times J_{\text{photo}}\ (A\ \text{cm}^{-2})}{\lambda\ (\text{nm}) \times I_{\text{inc}}\ (W\ \text{cm}^{-2})} \times 100. \quad (3)$$

Figure 6 represents the IPCE curve for the cell fabricated using synthesized ZnO powders sensitized by N719 dye, and the values are listed in Table 1. The maximum IPCE obtained was 46 % with cell fabricated by flower-like ZnO as photoanode in DSSCs.

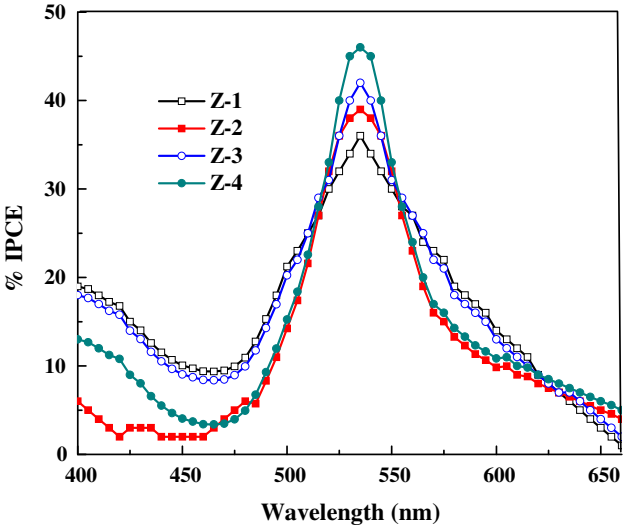

Fig. 6 Incident photon-to-current conversion efficiency (IPCE vs. λ) plots for different ZnO-N719/electrolyte/Pt DSSCs assembly

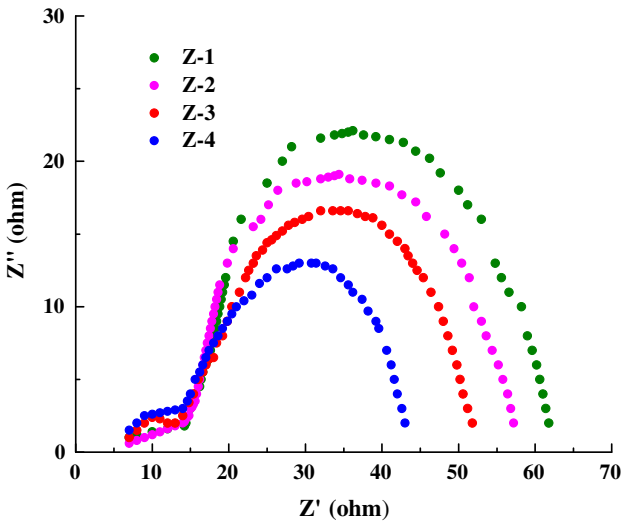

Fig. 7 Electrochemical impedance spectra of DSSCs made of different ZnO as photoanode in light sensitized by N719 dye in the frequency range of 10^{-2} to 10^5 Hz

EIS study

For investigating electron transport properties of ZnO/dye/electrolyte interface in DSSCs, the EIS has been used. In EIS, the study of semicircle in the middle frequency region is associated with the electron/charge transfer at ZnO/dye/electrode interface (Wang et al. 2005; Lee et al. 2008; Yanagida et al. 2009).

The EIS Nynquist plots of the DSSCs based on the ZnO/dye/electrolyte interface are shown in Fig. 7. According to the EIS spectra shown in Fig. 7, the charge-transfer resistance for ZnO/dye/electrolyte interface in light decreases with the decreasing semicircle diameter. The charge-transfer resistance decreases for the system using different

ZnOs as photoanode in the following trend: Z-4 > Z-3 > Z-2 > Z-1 at ZnO/dye/electrolyte interface.

Conclusion

In summary, different morphologies of ZnO powders have been synthesized successfully via surfactant-assisted precipitation routes. The different surfactants used in the synthesis provided different architectures for the ZnO as well as offered different surface areas. The pXRD for all ZnO nanostructure reveals the formation of single crystalline hexagonal phase. The optical study shows the blue shift than the bulk ZnO. The photovoltaic performances for the cell using these ZnO samples as photoanode was showing the cell efficiency trend Z-4 > Z-3 > Z-2 > Z-1. The Z-4 shows the highest efficiency than the others as it offers greater surface area for greater dye loading. The difference in efficiency is due to different surface areas, as particle size decreases surface area increases and dye loading also increases. The above efficiency trend was also supported by impedance study (EIS spectra) which shows the decrease in resistance in light for Z-4 sample which is more acute than the others. From this study, we can conclude that by modifying synthesis procedure one can get much better efficiency in future. From this study, we concluded that by varying surfactant we can easily tailor the shape, size, and morphology of ZnO and improve its performance as photoanode in DSSCs.

Acknowledgments Authors are grateful to the Department of Science and Technology and UGC, New Delhi for providing financial support to undertake this work.

References

Brinker CJ, Scherer GW (1990) Sol–gel Science: the physics and chemistry of sol–gel processing. Academic Press, San Deigo

Duong TT, Choi HJ, He QJ, Le AT, Yoon SG (2013) Enhancing the efficiency of dye sensitized solar cells with an SnO_2 blocking layer grown by nanocluster deposition. J Alloys Comp 561:206–210

Gratzel M (2003) Dye-sensitized solar cells. J Photochem Photobiol C Photochem Rev 4:145–153

Hagfeldt A, Grätzel M (1995) Light-induced redox reactions in nanocrystalline systems. Chem Rev 95:49–68

Hagfeldt A, Boschloo G, Sun L, Kloo L, Pettersson H (2010) Dye-sensitized solar cells. Chem Rev 110:6595–6663

Hu X, Heng B, Chen X, Wang B, Sun D, Sun Y, Zhou W, Tang Y (2012) Ultralong porous ZnO nanobelt arrays grown directly on fluorine-doped SnO_2 substrate for dye-sensitized solar cells. J Power Sources 217:120–127

Jennings JR, Ghicov A, Peter LM, Schmuki P, Walker AB (2008) Dye-sensitized solar cells based on oriented TiO_2 nanotube arrays: transport, trapping, and transfer of electrons. J Am Chem Soc 130:13364–13372

Kalyansundaramand K, Grätzel M (1998) Applications of functionalized transition metal complexes in photonic and optoelectronic device. Coord Chem Rev 177:347–414

Koch U, Fojtik A, Weller H, Henglein A (1985) Photochemistry of semiconductor colloids. Preparation of extremely small ZnO particles, fluorescence phenomena and size quantization effects. Chem Phys Lett 122:507–510

Kong FT, Dai SY, Wang KJ (2007) Review of recent progress in dye-sensitized solar cells. Adv Optoelectron 2007:1–13

Lee KM, Hu CW, Chen HW, Ho KC (2008) Incorporating carbon nanotubes in a low-temperature fabrication process for dye-sensitized Tio_2 solar cells. Sol Energy Mater Sol Cells 92:1628–1633

Meng XQ, Zhao DX, Zhang JY, Shan DZ, Lu YM, Liu YC, Fan XW (2005) Growth temperature controlled shape variety of ZnO nanowires. Chem Phys Lett 407:91–94

Meulenkamp EA (1998) Synthesis and growth of ZnO nanoparticles. J Phys Chem B 102:5566–5572

Nyffenegger RM, Craft B, Shaaban M, Gorer S, Erley G, Penner RM (1998) A hybrid electrochemical/chemical synthesis of zinc oxide nanoparticles and optically intrinsic thin films. Chem Mater 10:1120–1129

O'Regan B, Gratzel M (1991) Low-cost high-efficiency solar cell based on dye-sensitized colloidal TiO2 films. Nature 353:737–740

Pan ZW, Dai ZR, Wang ZL (2001) Nanobelts of semiconducting oxides. Science 291:1947–1949

Polo AS, Itokazu MK, Iha NYM (2004) Metal complex sensitizers in dye- sensitized solar cells. Coord Chem Rev 248:1343–1361

Sakai N, Miyasaka T, Murakami TN (2013) Efficiency enhancement of ZnO-based dye-sensitized solar cells by low-temperature $TiCl_4$ treatment and dye optimization. J Phys Chem C 117:10949–10956

Spanhel L, Anderson MA (1991) Semiconductor clusters in the sol–gel process—quantized aggregation, gelation, and crystal-growth in concentrated ZnO colloids. J Am Chem Soc 113:2826–2833

Umar A, Lee S, Lee YS, Nahm KS, Hahn YB (2005) Star-shaped ZnO nanostructures on silicon by cyclic feeding chemical vapor deposition. J Cryst Growth 277:479–484

Wahab R, Ansari SG, Kim YS, Seo HK, Shin HS (2007a) Room temperature synthesis of needle-shaped ZnO nanorods via sonochemical method. Appl Surf Sci 253:7622–7626

Wahab R, Ansari SG, Kim YS, Seo HK, Kim GS, Khang G, Shin HS (2007b) Low temperature solution synthesis and characterization of ZnO nano-flowers. Mater Res Bull 42:1640–1648

Wahab R, Ansari SG, Kim YS, Khang G, Shin HS (2008) Effect of hydroxylamine hydrochloride on the floral decoration of zinc oxide synthesized by solution method. Appl Surf Sci 254:2037–2042

Wang Q, Moser JE, Gratzel M (2005) Electrochemical impedance spectroscopic analysis of dye-sensitized solar cells. J Phys Chem B 109:14945–14953

Xu F, Sun L (2011) Solution-derived ZnO nanostructures for photoanodes of dye-sensitized solar cells. Energy Environ Sci 4:818–841

Xu F, Zhang X, Wu Y, Wu D, Gao Z, Jiang K (2013) Facile synthesis of TiO_2 hierarchical microspheres assembled by ultrathin nanosheets for dye-sensitized solar cells. J Alloys Comp 574:227–232

Yanagida S, Yu YH, Manseki K (2009) Iodine/iodide-free dye-sensitized solar cells. Acc Chem Res 42:1827–1838
Zhang Q, Cao G (2011) Nanostructured photoelectrodes for dye-sensitized solar cells. Nano Today 6:91–109
Zhang J, Sun L, Yin J, Su H, Liao CS, Yan C (2002) Control of ZnO morphology via a simple solution route. Chem Mater 14:4172–4177
Zhang Q, Dandeneau CS, Zhou X, Cao G (2009) ZnO nanostructures for dye-sensitized solar cells. Adv Mater 21:4087–4108